Anal Bioanal Chem
DOI 10.1007/s00216-016-9480-5

RESEARCH PAPER

First report on hemoglobin electrostatic immobilization on WO_3 nanoparticles: application in the simultaneous determination of levodopa, uric acid, and folic acid

Javad Ghodsi[1] · **Amir Abbas Rafati**[1] · **Yalda Shoja**[1]

Received: 8 January 2016 / Revised: 15 February 2016 / Accepted: 10 March 2016

Abstract This work describes the first report about the simultaneous determination of levodopa (L-DOPA) with folic acid (FA) and uric acid (UA) based on electrocatalytic oxidation of L-DOPA with peroxidase properties of hemoglobin (Hb) in the presence of H_2O_2 as Hb activator. Bovine Hb was electrostatically immobilized on WO_3 nanoparticles (WO_3NPs) in pH between Hb and WO_3NP isoelectric points, and subsequently, a carbon paste electrode (CPE) was modified with the obtained WO_3NPs-Hb and multiwalled carbon nanotubes (MWCNTs). The resulting biosensor supplied a sensitive and suitably stable biosensor for the simultaneous determination of L-DOPA, UA, and FA. The obtained linear range and detection limit for L-DOPA, UA, and FA were completely acceptable, and the biosensor response time for these molecules was relatively short so that it reaches about 95 % of its maximum response in less than 10 s. The applicability of the current biosensor was confirmed with the determination of L-DOPA in the presence of fixed amounts of FA and UA in some real samples by the standard addition method.

Keywords Biosensor · Hemoglobin · Simultaneous determination · Levodopa · Folic acid · Uric acid

Introduction

L-DOPA [(3,4-dihydroxyphenylalanine) propionic acid], a catecholamine drug, is mostly used in the treatment of Parkinson's disease. People who have Parkinson's disease are suffering from deficiency of dopamine (the most important neurotransmitter in the nervous system) in the brain. L-DOPA is used to increase dopamine in the brain, which reduces the symptoms of Parkinson's disease and provides symptomatic relief at the initial stages of the disease. Considering the serious side effects due to chronic administration of this drug in Parkinson's patients and also achieving its better curative effects, the determination of L-DOPA has attracted many attention in recent years [1–3]. A significant number of reports on L-DOPA determination have been provided by applying gas chromatography (GC) [4], high-performance liquid chromatography (HPLC) [5], circular dichroism [6], chemiluminescence [7], UV-Vis spectrophotometry [8], potentiometry [9], spectrofluorimetry [10], flow injection analysis (FIA) [11], capillary electrophoresis [12], ^{1}H NMR [13], fluorescence [14], catalytic anodic stripping voltammetry [15], and amperometric method [16]. Among all developed methods, those which are based on electrochemical methods have several advantages such as sensitivity, reproducibility, cost effectiveness, and ease of use [1, 17–21].

Uric acid (UA), the main final product of purine oxidation, exists in biological fluids such as blood or urine and is largely excreted by the kidneys. A high concentration level of UA in the human body may cause diseases such as hyperuricemia, gouty arthritis, and the Lesch-Nyan disease. Also, it may be associated with several diseases such as hypertension, pneumonia, type 2 diabetes, cardiovascular disease, and kidney damage [22–25]. The abovementioned points can be regarded as reasons for the high importance of UA determination in biological samples.

Folic acid (FA) is another important biomolecule that was measured with L-DOPA in this work. FA, also a water-soluble vitamin B, is essential during the period of cell growth and division. FA paucity in human body fluids could result in

✉ Amir Abbas Rafati
aa_rafati@basu.ac.ir; rafati_aa@yahoo.com

[1] Department of Physical Chemistry, Faculty of Chemistry, Bu-Ali Sina University, P.O.Box 65174, Hamedan, Iran

Published online: 23 March 2016

some diseases such as neurosis, mentality devolution, leucopoenia, megaloblastic anemia, cardiovascular disease, growth weakness, and colorectal cancer [26–30]. Thus, the measurement of this compound in biological fluids is also so important. The co-existence of UA and FA in different real samples was verified, and many works have been concerned with the simultaneous determination of these two compounds [31–33], but as far as we know, there is only one report on the simultaneous determination of L-DOPA, UA, and FA [1]. The current work provides the first report on the simultaneous determination of L-DOPA, UA, and FA based on electrocatalytic oxidation of L-DOPA with bovine Hb immobilized on tungsten oxide nanoparticles (WO_3NPs).

Enzymatic biosensors for catecholamines like L-DOPA and other phenolic compounds are mainly fabricated by applying peroxidase enzymes such as tyrosinase [34, 35] and laccase [36, 37]. These enzymatic biosensors have some advantages such as high sensitivity and selectivity but also have some disadvantages like high price and low stability. Hb with peroxidase properties nominates itself as low price and an abundant alternative for peroxidase enzymes. However, there are only few reports on the determination of phenolics or catecholamines using Hb-modified biosensors [38, 39].

WO_3 is an N-type semiconductor with a band gap of 2.5 eV with some interesting optical and electrical properties which enable its application in many fields as photocatalysts [40], electrochromic devices [41], solar energy devices [42], gas sensors [43], and field-emission devices [44]. Specially, its application in developing sensing materials has attracted many attention based on a reversible change of conductivity [45]. Several constructions of sensors using WO_3 have been reported, for example, sensors for NO, NO_2, acetone, and H_2S [46–49]. However, to the best of our knowledge, there is only one paper on sensor development by applying Hb with WO_3 support that was reported using Hb immobilized on WO_3 nanowires in a nitrite sensor fabrication [50], and up to now, no work has been reported about applying WO_3 in the development of a biosensor for the determination of a catecholamine like L-DOPA or FA and UA. Interestingly, the electrocatalytical properties of WO_3 have been used to develop several sensors as well as to facilitate the electron transport of enzymes [51], and we introduced this metal oxide as a novel and proper support for enzymes applied in various enzymatic biosensors.

In this work, bovine Hb was electrostatically immobilized on WO_3NPs, and the prepared WO_3NPs-Hb with multiwalled carbon nanotube were applied to modify the carbon paste electrode (CPE). The fabricated biosensor showed excellent electrocatalytical properties in the simultaneous determination of L-DOPA, FA, and UA. The developed biosensor also showed high sensitivity and stability, low detection limit, vast linear range, and short time response. Also, the applicability of the biosensor was confirmed with L-DOPA determination in the presence of FA and UA in real samples.

Experimental

Chemicals

WO_3NPs with an average diameter of 50 nm and multiwalled carbon nanotubes (MWCNTs) were purchased from Neutrino Co. (Iran). Bovine Hb was purchased from Sigma-Aldrich Co. L-DOPA was purchased from Darou Pakhsh Co. (Iran). All the other reagents were of analytical grade and used without further purification. All electrochemical measurements were performed at 50 mM in phosphate buffer (PB) of pH 7 that contains an optimized amount of H_2O_2 (200 μM) for the initial activation of Hb. All experiments were carried out at room temperature (25 ± 0.1 °C). Electrochemical measurements were performed at a potential scan rate of 100 mV s^{-1} unless otherwise stated.

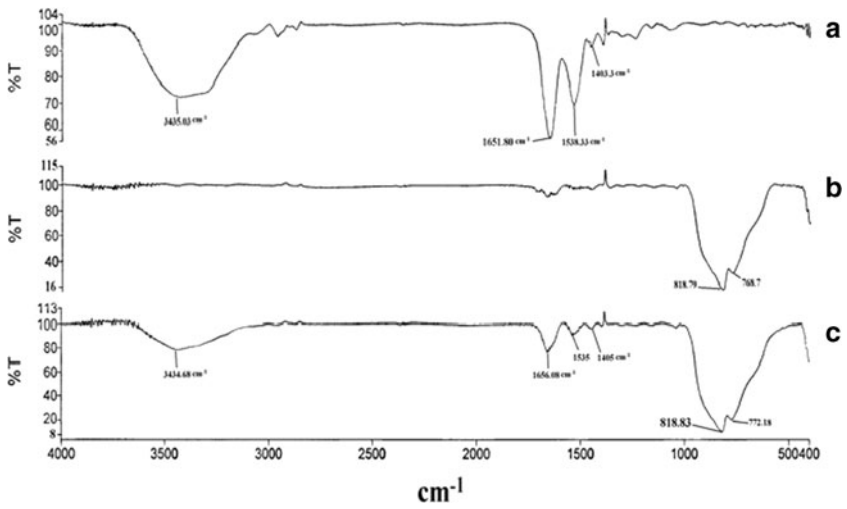

Fig. 1 FT-IR spectrums of **a** Hb, **b** WO_3, and **c** WO_3NPs-Hb

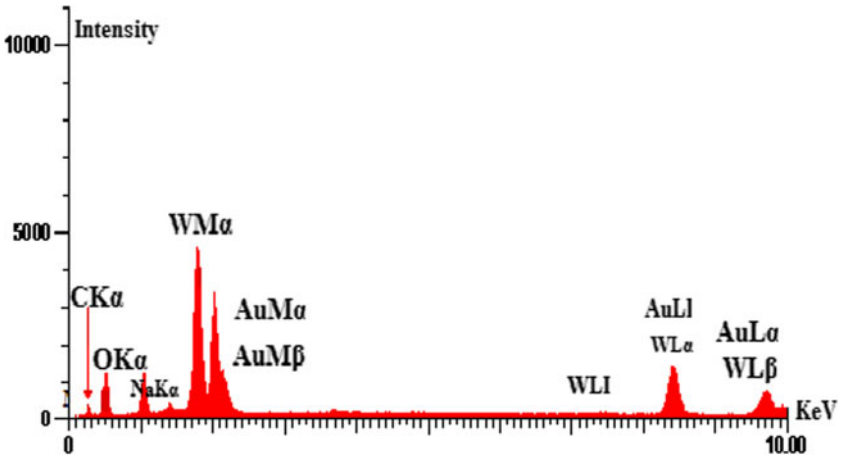

Fig. 2 SEM-EDX analysis for WO_3NPs-Hb

Apparatus

Voltammetric experiments were carried out with a computer-controlled μ-Autolab modular electrochemical system (PGSTAT101, purchased from Metrohm Co.), driven with NOVA software (upgrade 1.10). A three-electrode system was used with the CPE electrode modified with WO_3NPs-Hb and MWCNTs, called CPE/WO_3NPs-Hb/MWCNTs, as the working electrode; an Ag/AgCl (saturated potassium chloride) as the reference electrode; and a platinum foil as the counter electrode. The counter and reference electrodes were from Azar Electrode Co. (Iran). Spectrometry measurements were performed with a UV-Vis spectrophotometer (Analytik Jena AG, from Analytik Jena Co.). All solutions were deoxygenated with pure nitrogen for at least 2 min. All electrochemical measurements were performed in a PB buffer of pH 7.

Preparation of the CPE/WO_3NPs-Hb/MWCNT electrode

Firstly, bovine Hb was treated with WO_3NPs to electrostatically immobilize WO_3NPs, and WO_3NPs-Hb was obtained. To achieve this aim, WO_3NPs were incubated with Hb in phosphate buffer at pH 5. Isoelectric points of Hb and WO_3NPs are about 7 and 1.5, respectively [38, 52]; so, in the previously mentioned pH, positively charged Hb can immobilize onto the negatively charged WO_3NPs. Optimized experimental parameters including pH, incubation time, and Hb concentration for maximum Hb immobilization were found and applied for the next preparation of WO_3NPs-Hb. The amount of immobilized Hb on WO_3NPs was evaluated from the difference in UV-Vis absorbance of Hb solution in about 405 nm before and after treating with WO_3NPs. UV-Vis absorbance of Hb was related to Hb concentration by applying a standard calibration curve for Hb (obtained as milligrams per milliliter of Hb vs. UV-Vis absorbance at ~405 nm). Modified CPE was initially prepared by homogenization of 65 mg of graphite powder, 15 mg of MWCNTs, and 10 mg of just prepared WO_3NPs-Hb in a small glass oven. Then, 25 mg of mineral oil was subsequently added to this mixture in the oven and mixed for several minutes to produce the final paste. The modified carbon paste was packed into the tip of a 1-ml insulin plastic syringe, and a copper wire was inserted to obtain the

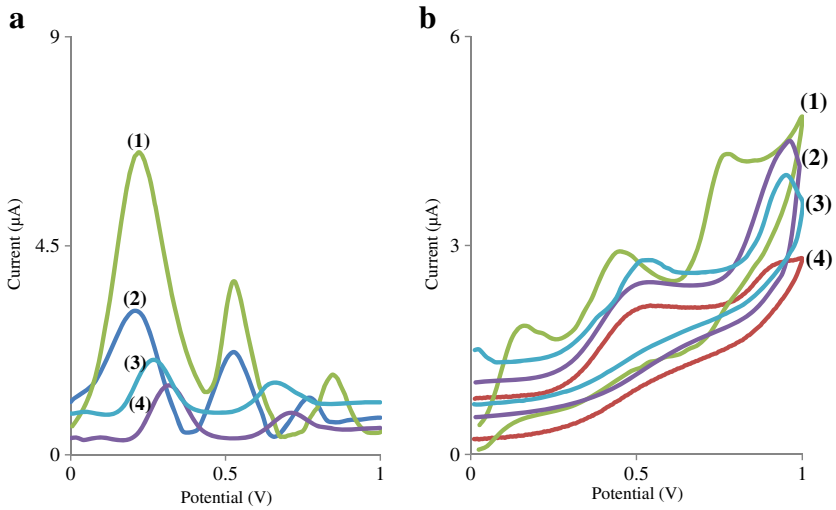

Fig. 3 **a** DPVs of a buffer solution containing 1 mM of L-DOPA, UA, and FA by *1* CPE/WO_3NPs-Hb/MWCNT, *2* CPE/Hb/MWCNT, *3* CPE/WO_3NPs/MWCNT, and *4* CPE/MWCNT electrodes as work electrode. **b** CVs of buffer containing 40 mM FA, 10 mM UA, and 3 mM L-DOPA by *1* CPE/WO_3NPs-Hb/MWCNT, *2* CPE/Hb/MWCNT, *3* CPE/WO_3NPs/MWCNT, and *4* CPE/MWCNT electrodes

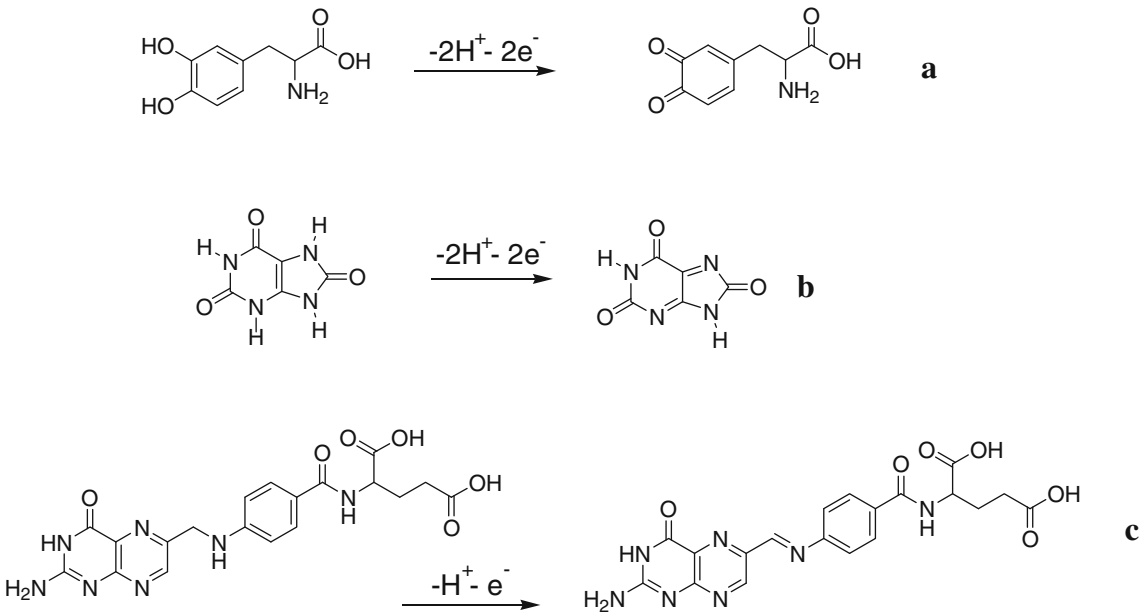

Scheme 1 Equation for oxidation of L-DOPA (**a**), UA (**b**), and FA (**c**) at surface electrode

external electric contact. Finally, the electrode surface was polished with a piece of soft paper to prepare the electrode for the next electrochemical experiments.

Results and discussion

Hb immobilization on WO_3NPs

Bovine Hb immobilization on WO_3NPs was investigated by SEM-EDX and FT-IR techniques. Figure 1 shows the FT-IR spectra of (a) Hb, (b) WO_3NPs, and (c) WO_3NPs-Hb. Peaks of about 818 and 770 cm^{-1} in spectrums b and c are assigned to the W-O units and the bridging oxygen stretching vibrations of O-W-O, respectively [53]. Characteristic Hb peaks at 1655, 1535, and 1405 cm^{-1} in spectrum a are assigned to the amide I, amide II, and C-N stretching modes, respectively [38]. The presence of Hb characteristic peaks in WO_3NPs-Hb FT-IR spectrum c strongly verifies the attachment of Hb molecules onto WO_3NPs.

Furthermore, Hb immobilization on WO_3NPs was verified with SEM-EDX analysis. The resulting spectrum is shown in Fig. 2. Characteristic peaks for tungsten can be seen at about 1800, 7500, 8500, and 9700 keV. Also, Au peaks in the spectrum refer to gold coating of the WO_3MNPs-Hb sample prior to SEM-EDX analysis. The carbon peak at about 250 keV, which is marked with an arrow, is corresponding to the carbon content of Hb immobilized onto WO_3NPs.

Important experimental parameters including pH, incubation time, and Hb concentration that affect Hb immobilization on WO_3NPs were investigated, and the optimized parameters were determined. As expected, the optimized pH obtained was about 5 which is approximately between that of WO_3 and Hb isoelectric points. The optimized incubation time and Hb

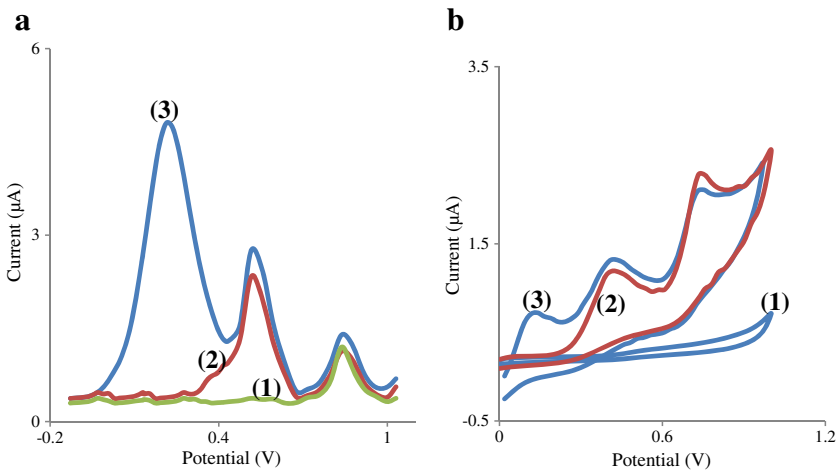

Fig. 4 **a** DPVs of buffers containing *1* 0.7 mM FA, *2* 0.7 mM FA + 1 mM UA, and *3* 0.7 mM FA + 1 mM UA + 0.7 mM L-DOPA. **b** CVs of buffer (*1*), 0.7 mM FA + 1 mM UA (*2*), and 0.7 mM FA + 1 mM UA + 0.7 mM L-DOPA (*3*)

concentration for maximum immobilization were determined to be about 25 min and 1 mg/ml of Hb, respectively. These optimized amounts were applied to the next WO_3NPs-Hb preparation.

Prior to electrochemical investigations, another critical parameter affecting biosensor performance, the amount of H_2O_2 added, was optimized. It is verified that low amounts of H_2O_2 can result in the low sensitivity of the biosensor, and its high amount can inactivate the Hb applied in the biosensor. The response of the biosensor to a fixed amount of L-DOPA was evaluated in the presence of different amounts of H_2O_2, and the H_2O_2 amount corresponding to the highest response (highest L-DOPA anodic peak current) was regarded as the optimized amount for H_2O_2 concentration. This amount was found to be about 200 μM. It is also verified that this optimized amount is nearly independent from the analyte concentration and most probably depends only on the amount of Hb applied in biosensor fabrication.

Electrochemical investigations

All electrochemical experiments in this section were carried out by differential pulse voltammetry (DPV) and cyclic voltammetry (CV). The electrochemical response of the fabricated biosensor to L-DOPA, UA, and FA was compared to CPE/MWCNT, CPE/WO_3NPs/MWCNT, and CPE/Hb/MWCNT electrodes with CV and DPV voltammograms. Results are shown in Fig. 3. Figure 3a shows the DPV

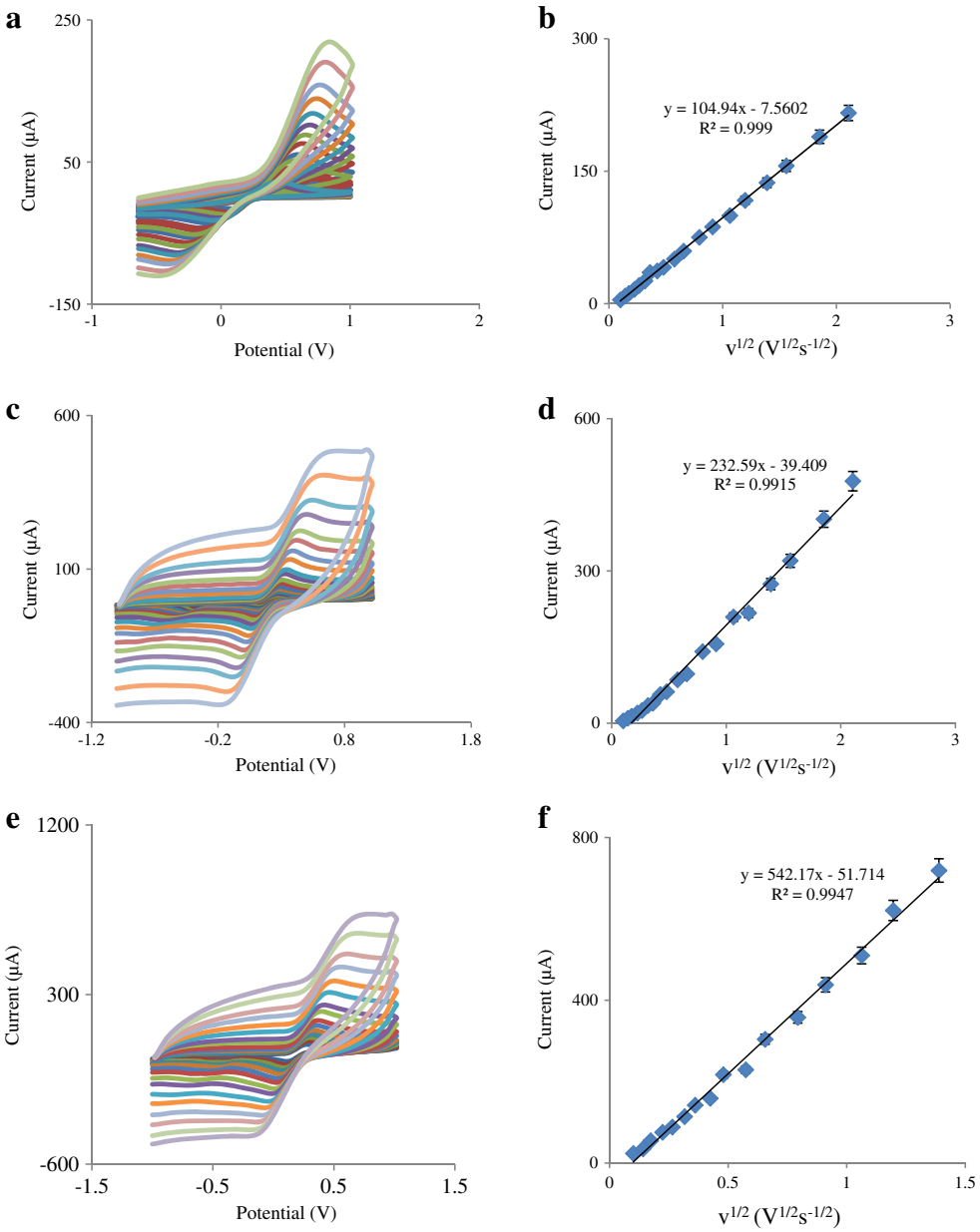

Fig. 5 CVs for 1 mm $K_3Fe(CN)_6$ and 0.1 M KCl, obtained by **a** CPE, **c** CPE/MWCNT, and **e** CPE/WO_3NPs-Hb/MWCNT electrodes as work electrodes in potential scan rates of 10–4400 mV s^{-1}. Anodic peak current vs. square root of potential scan rate plots for **b** CPE, **d** CPE/MWCNT, and **f** CPE/WO_3NPs-Hb/MWCNT electrodes

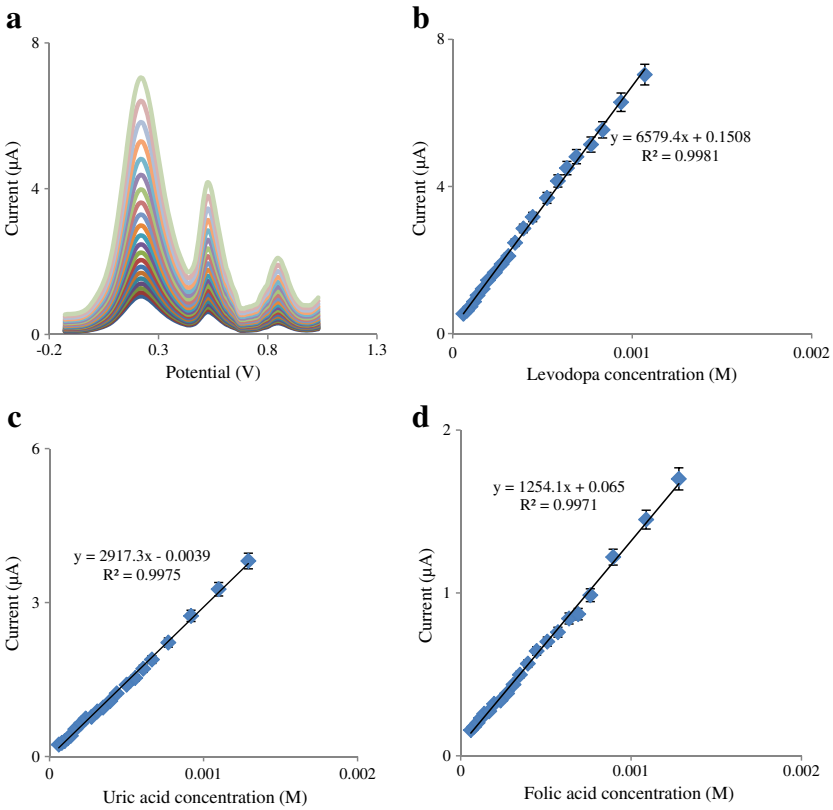

Fig. 6 **a** DPVs of buffer with successive addition of FA, UA, and L-DOPA. Calibration curves for L-DOPA (**b**), UA (**c**), and FA (**d**)

voltammograms of a phosphate buffer containing 1 mM of L-DOPA, UA, and FA obtained by (1) CPE/WO_3NPs-Hb/MWCNTs, (2) CPE/Hb/MWCNTs, (3) CPE/WO_3NPs/MWCNTs, and (4) CPE/MWCNTs as work electrodes. As shown in Fig. 3a, there are three well-defined anodic peaks corresponding to L-DOPA, UA, and FA (anodic peaks corresponded to L-DOPA, UA, and FA from low to high potential, respectively) only in Hb containing electrodes including CPE/WO_3NPs-Hb/MWCNTs and CPE/Hb/MWCNTs. This clearly shows the role of Hb in the possibility of simultaneous determination of analytes. Moreover, CPE/WO_3NPs-Hb/MWCNTs show significantly higher sensitivity to analytes especially to L-DOPA in comparison to CPE/Hb/MWCNTs. This shows the synergic effect of WO_3NPs and Hb in L-DOPA oxidation at the electrode surface. DPVs obtained by CPE/WO_3NPs/MWCNTs and CPE/MWCNTs are shown in voltammograms (3) and (4), respectively, which show only two anodic peaks. Anodic peaks in lower potential in these two DPVs are mainly due to L-DOPA oxidation. As clearly seen, L-DOPA anodic peaks in these current DPVs appeared in higher potential than Hb containing electrodes. This confirms the electrocatalytic role of Hb in electrocatalytic oxidation of L-DOPA. The mechanism of electrocatalytic oxidation of a catecholamine (L-DOPA) with Hb in the presence of H_2O_2 was explained in our previously published work about dopamine determination [38] as follows: at first, the heme group of immobilized Hb on WO_3 nanoparticle was oxidized by H_2O_2 added to the analyte solution; then, the oxidized heme easily oxidized the L-DOPA and then the reduced Hb is oxidized on the electrode surface and the resulting anodic peak current can directly relate to L-DOPA concentration. Also, greater oxidation peak currents corresponding to UA and FA show the good performance of the electrode modified with WO_3NPs-Hb in oxidation of these two molecules. Scheme 1 shows the equation for the oxidation of L-DOPA (a), UA (b), and FA (c) at the surface electrode. The response of the modified electrode was also compared with the three electrodes of

Table 1 Linear range, detection limits, and regression linear equation obtained for L-DOPA, UA, and FA

Compound	L-DOPA	UA	FA
Linear range (μM)	60–1070	60–1290	60–1280
Detection limit (μM)	0.25	0.11	0.07
Regression equation/correlation coefficient	$I_{an} = 6579.4C + 0.1508$ $R^2 = 0.9981$	$I_{an} = 2917.3C - 0.0039$ $R^2 = 0.9975$	$I_{an} = 0.0013C + 0.065$ $R^2 = 0.9971$

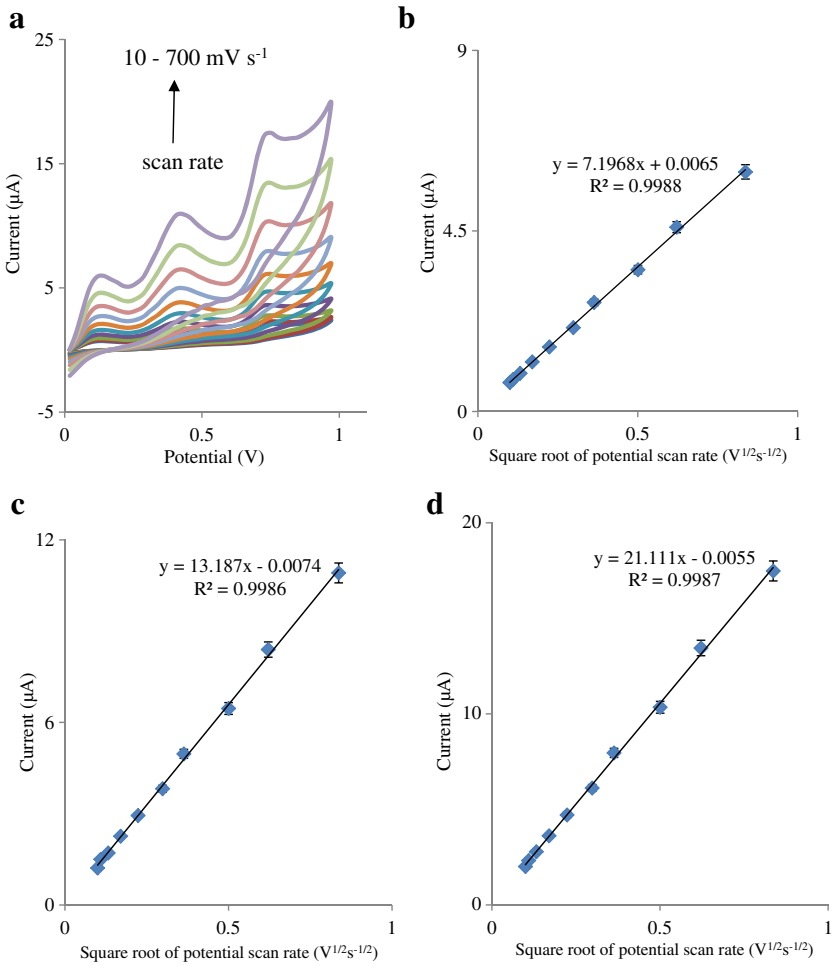

Fig. 7 **a** CVs of buffer containing 0.4 mM L-DOPA, 1.5 mM UA, and 5 mM FA in potential scan rate of 10 to 700 mV s^{-1}. Anodic peak current vs. square root of potential scan rate for L-DOPA, UA, and FA in **b**–**d**, respectively

CPE/Hb/MWCNTs, CPE/WO_3NPs/MWCNTs, and CPE/MWCNTs with CV voltammograms. The results are shown in Fig. 3b. As can be seen, there are three well-defined oxidation peaks in CV obtained by the developed biosensor (CPE/WO_3NPs-Hb/MWCNTs as the work electrode), while only two oxidation peaks are seen in CV corresponding to CPE/Hb/MWCNTs, CPE/WO_3NPs/MWCNTs, and CPE/MWCNTs that are possibly related to the oxidation of UA and FA. For more investigation of the simultaneous determination of these compounds by the developed biosensor, buffers containing FA, FA + UA, and FA + UA + L-DOPA were investigated by DPV and CV voltammograms.

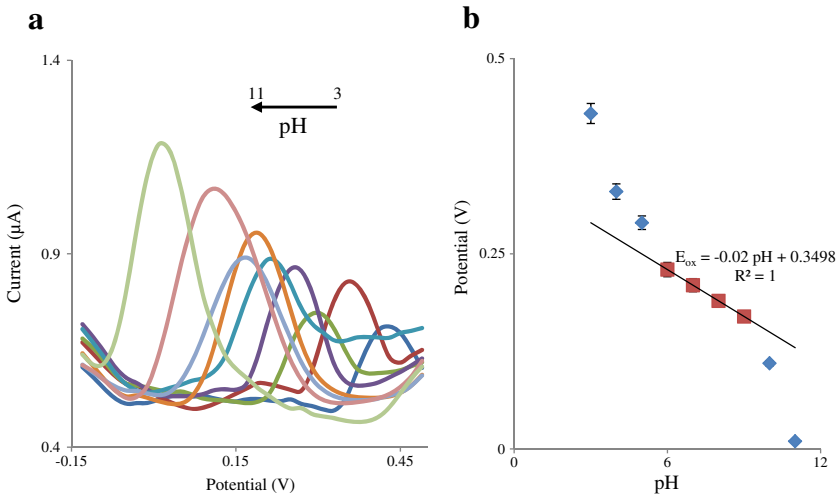

Fig. 8 **a** DPVs of 0.1 mM L-DOPA (with 0.1 mM of UA and FA) in pH values 3–11 (UA and FA anodic peaks have been deleted). **b** Plot for anodic potentials of L-DOPA vs. pH

Table 2 L-DOPA determination in real samples in the presence of fixed amounts of UA and FA (200 μM)

Sample	Added (μM)	Expected (μM)	Found (μM)—the mean of three measured values	Recovery (%)
Serum	100.0	100.0	104.7	104.7
	150.0	150.0	146.7	97.8
	200.0	200.0	210.5	105.3
Urine	100.0	100.0	96.2	96.2
	150.0	150.0	144.0	96.0
	200.0	200.0	204.8	102.4

Results are shown in Fig. 4. As shown in the CV and DPV voltammograms, the oxidation peak currents of these three compounds have only a slight effect on each other so L-DOPA can be simultaneously measured with UA and FA by applying the developed biosensor as work electrode without any significant interference from FA or UA.

Another electrochemical investigation was the calculation of the active surface area of the developed biosensor and its comparison with two electrodes namely CPE and CPE/MWCNTs. The active surface area of the electrodes was calculated according to the slope of the I_{pa} vs. $\nu^{1/2}$ plot for a known concentration of $K_4Fe(CN)_6$, based on the Randles-Sevcik equation:

$$I_{pa} = 2.69 \times 10^5 n^{3/2} A D_R^{1/2} \nu^{1/2} C_0$$

where I_{pa} refers to the anodic peak current, n the electron transfer number, A the surface area of the electrode, D_R the diffusion coefficient, C_0 the concentration of $K_4Fe(CN)_6$, and ν the potential scan rate. For 1.0 mM of $K_4Fe(CN)_6$ in 0.10 M of KCl electrolyte with $n = 1$ and $D_R = 7.6 \times 10^{-6}$ cm s^{-1}, the microscopic areas of the electrodes were calculated by the slope of the I_{pa}–$\nu^{1/2}$ curve. They were 0.135, 0.027, and 0.067 mm^2 for (a) CPE, (b) CPE/MWCNT, and (c) CPE/WO_3NPs-Hb/MWCNT electrodes, respectively. These results show the larger active surface area for the developed biosensor than the two other mentioned electrodes and, consequently, show more capability of the developed biosensor in the oxidation of the mentioned analytes on its surface. Comparison of the obtained values for the electrode active surface area reveals the crucial role of WO_3NPs-Hb in increasing the active sites for analyte oxidation at the electrode surface. The results of this section are shown in Fig. 5.

Figure 5 shows the CV voltammograms for 1-mm $K_3Fe(CN)_6$ and 0.1-M KCl, obtained by (a) CPE, (c) CPE/MWCNT, and (e) CPE/WO_3NPs-Hb/MWCNT electrodes as work electrodes in the potential scan rates of 10–4400 mV s^{-1}, and their respective anodic peak current vs. square root of potential scan rate plots are shown for CPE (b), CPE/MWCNT (d), and CPE/WO_3NPs-Hb/MWCNT (f) electrodes.

The most satisfactory result of this work is the standard calibration curves obtained for the simultaneous measurement of the mentioned analytes. For the preparation of the standard calibration curve, a stock solution with distinct amounts of UA, FA, and L-DOPA was prepared and successively added to phosphate buffer, and DPVs were measured. The respective DPV voltammograms (a) and the obtained standard calibration curves for L-DOPA (b), UA (c), and FA (d) are shown in Fig. 6. Linear range, sensitivity, and detection limit for these measured compounds are shown in Table 1. All of these analytical amounts for FA, UA, and L-DOPA that are in

Table 3 Comparison of the performance of our electrode in the simultaneous L-DOPA detection with other recently reported works

Basic electrode	Technique	Modifier	Linear range	Detection limit	Other analyte	Reference
GCE	DPV/CV	Graphene	1–16 μM	0.8 μM	Carbidopa	[54]
CPE	DPV/CV	Poly(methyl orange) film	20–100 μM and 100–800 μM	3.7 μM	Uric acid and ascorbic acid	[55]
GCE	DPV/CV	Quercetin-functionalized MWCNTs	0.90–85.0 μM	0.381 μM	Uric acid and tyramine	[19]
CPE	DPV/CV	CNT/ferrocene	2–500 μM	1.2 μM	–	[56]
CPE	DPV/CV	Lead dioxide immobilized in a polyester resin	260 μM–1.2 mM	25 μM	Carbidopa	[57]
GCE	SWV/ads SWV	Nafion carbon nanotubes	0.25–10 μM/1–10 μM	0.52 nM	Ropinirole	[17]
GCE	DPV/SWV	–	0.5–2 μM/1–20 μM	0.11 μM	Ropinirole	[58]
CPE	DPV/CV	WO_3NPs-Hb	60–1070 μM	0.25 μM	Uric acid and folic acid	Our work

simultaneous measurement are completely acceptable compared to other reported works.

The effect of potential scan rate on the oxidation peak currents of FA, UA, and L-DOPA was also investigated by CV voltammograms in the potential scan rate of 10 to 700 mV s^{-1}. The corresponding CV voltammograms are shown in Fig. 7a. Anodic peak current vs. square root of the potential scan rate was plotted for L-DOPA, UA, and FA in panels b, c, and d, respectively, in Fig. 7. The results showed that the anodic peak currents for all three compounds increased linearly with the increase in the square root of scan rate. These linear dependences between anodic peak currents and the root of potential scan rate show that the electrode process is mainly controlled under the diffusion step for the oxidation of all three compounds on the modified electrode surface.

The effect of pH in the electrocatalytical oxidation of FA, UA, and L-DOPA at the electrode surface was also investigated with DPV measurements in different pH values, but to avoid sloppy voltammograms, only anodic peak currents for L-DOPA are shown in Fig. 8a. As can be seen in this figure, the oxidation peak current for L-DOPA was negatively shifted by increasing pH that was completely expected with regard to the oxidation chemical equation of L-DOPA. Oxidation potential is linearly related to pH in the range of 6–9 by the equation $E_{ox} = -0.02\ pH + 0.3498$ and excellent correlation coefficient of 1, where E_{ox} refers to the oxidation potential of L-DOPA. The plot for E_{ox} vs. pH is shown in Fig. 8b.

The applicability of the developed electrode was verified with L-DOPA determination in real samples including urine and serum containing 200 μM of FA and UA by standard addition method. The results are summarized in Table 2, and as shown in this table, recovery is between 96.0 and 105.3, which is very satisfactory for accurate drug determination in real samples. The stability of the developed biosensor was also investigated, and results showed that it was suitably stable for 16 days if stored at 4 °C. Moreover, other studies showed the biosensor to have a short response time to the mentioned analytes so that it reached about 95 % of its maximum response at 5, 9, and 7 s to L-DOPA, UA, and FA, respectively.

Finally, the performance of the developed biosensor was compared to other recently reported work on electrochemical simultaneous determination of L-DOPA with compounds like as UA, FA, and so on. As shown in Table 3, our biosensor linear range and the detection limit for L-DOPA determination in the presence of two other analytes are very acceptable.

Conclusion

The current work reports the first application of WO_3 nanoparticles in the development of a biosensor for catecholamine. The described work provided a novel biosensor for the successful simultaneous determination of L-DOPA, UA, and FA based on electrocatalytic oxidation with hemoglobin immobilized onto WO_3 nanoparticles. Sensitivity, response time, stability, linear ranges, and detection limits achieved by this biosensor were completely acceptable. Also, the successful detection of L-DOPA in the presence of UA and FA in urine and serum verifies the good applicability of the developed biosensor in real samples. This work also introduces WO_3 nanoparticles as a suitable support for hemoglobin or other redox enzymes applied in enzymatic biosensor purposes.

Acknowledgments The authors greatly acknowledge Bu-Ali Sina University for the financial support from the Grant Research Council.

Compliance with ethical standards

Conflict of interest The authors declare that they have no conflict of interest.

References

1. Benvidi A, Dehghani-Firouzabadi A, Mazloum-Ardakani M, Mirjalili B-BF, Zare R. Electrochemical deposition of gold nanoparticles on reduced graphene oxide modified glassy carbon electrode for simultaneous determination of levodopa uric acid and folic acid. J Electroanal Chem. 2015;736:22–9.
2. Babaei A, Taheri AR, Farahani IK. Nanomolar simultaneous determination of levodopa and melatonin at a new cobalt hydroxide nanoparticles and multi-walled carbon nanotubes composite modified carbon ionic liquid electrode. Sens Actuators B. 2013;183:265–72.
3. Chen X, Zhang J, Zhai H, Chen X, Hu Z. Determination of levodopa by capillary zone electrophoresis using an acidic phosphate buffer and its application in the analysis of beans. Food Chem. 2005;92:381–6.
4. Hansson C, Agrup G, Rorsman H, Rosengren A-M, Rosengren E, Edholm L-E. Analysis of cysteinyldopas, dopa, dopamine, noradrenaline and adrenaline in serum and urine using high-performance liquid chromatography and electrochemical detection. J Chromatogr B. 1979;162:7–22.
5. Karimi M, Carl JL, Loftin S, Perlmutter JS. Modified high-performance liquid chromatography with electrochemical detection method for plasma measurement of levodopa, 3-O-methyldopa, dopamine, carbidopa and 3,4-dihydroxyphenyl acetic acid. J Chromatogr B. 2006;836:120–3.
6. Chunyi S. Application of circular dichroism in pharmaceutical analysis—I. Quantitative analysis of artemisinine and laevodopa in "laevodopa et benserazide". Chin J Anal Chem. 1992;10:011.
7. Yao D, Vlessidis AG, Evmiridis NP. Monitoring reactive oxygen species in vivo using microdialysis sampling and chemiluminescence detection as an alternative global method for determination of total antioxidant capacity. Anal Chim Acta. 2002;467:133–44.
8. Grünhut M, Centurión ME, Fragoso WD, Almeida LF, de Araújo MCU, Band BSF. Flow-batch technique for the simultaneous enzymatic determination of levodopa and carbidopa in pharmaceuticals using PLS and successive projections algorithm. Talanta. 2008;75:950–8.

9. Badawy S, Issa Y, Tag-Eldin A. Potentiometric determination of L-dopa, carbidopa, methyldopa and aspartame using a new trinitrobenzenesulfonate selective electrode. Electroanalysis. 1996;8:1060–4.
10. Aydoğmuş Z. Highly sensitive and selective spectrophotometric and spectrofluorimetric methods for the determination of ropinirole hydrochloride in tablets. Spectrochim Acta A. 2008;70:69–78.
11. Marcolino-Junior LH, Teixeira MF, Pereira AV, Fatibello-Filho O. Flow injection determination of levodopa in tablets using a solid-phase reactor containing lead (IV) dioxide immobilized. J Pharm Biomed Anal. 2001;25:393–8.
12. Nezhad MH, Tashkhourian J, Khodaveisi J. Sensitive spectrophotometric detection of dopamine, levodopa and adrenaline using surface plasmon resonance band of silver nanoparticles. J Iran Chem Soc. 2010;7:S83–91.
13. Talebpour Z, Haghgoo S, Shamsipur M. 1H nuclear magnetic resonance spectroscopy analysis for simultaneous determination of levodopa, carbidopa and methyldopa in human serum and pharmaceutical formulations. Anal Chim Acta. 2004;506:97–104.
14. Pagani AP, Cabezón MA, Ibanez GA. Simultaneous kinetic-spectrofluorometric determination of levodopa and carbidopa using partial least-squares regression. Anal Sci. 2009;25:633–8.
15. Hosseini M, Faraji M, Momeni M, Ershad S. An innovative electrochemical approach for voltammetric determination of levodopa using gold nanoparticles doped on titanium dioxide nanotubes. Microchim Acta. 2001;172:103–8.
16. Zhang L, Chen G, Hu Q, Fang Y. Separation and determination of levodopa and carbidopa in composite tablets by capillary zone electrophoresis with amperometric detection. Anal Chim Acta. 2001;431:287–92.
17. Sadiković M, Nigović B, Jurić S, Mornar A. Voltammetric determination of ropinirole in the presence of levodopa at the surface of a carbon nanotubes based electrochemical sensor in pharmaceuticals and human serum. J Electroanal Chem. 2014;733:60–8.
18. Babaei A, Taheri AR, Aminikhah M. Nanomolar simultaneous determination of levodopa and serotonin at a novel carbon ionic liquid electrode modified with $Co(OH)_2$ nanoparticles and multi-walled carbon nanotubes. Electrochim Acta. 2013;90:317–25.
19. Raoof JB, Ojani R, Amiri-Aref M, Baghayeri M. Electrodeposition of quercetin at a multi-walled carbon nanotubes modified glassy carbon electrode as a novel and efficient voltammetric sensor for simultaneous determination of levodopa, uric acid and tyramine. Sens Actuators B. 2012;166:508–18.
20. Mazloum-Ardakani M, Taleat Z, Khoshroo A, Beitollahi H, Dehghani H. Electrocatalytic oxidation and voltammetric determination of levodopa in the presence of carbidopa at the surface of a nanostructure based electrochemical sensor. Biosens Bioelectron. 2012;35:75–81.
21. Mazloum-Ardakani M, Beitollahi H, Sheikh-Mohseni MA, Naeimi H. Simultaneous determination of levodopa and carbidopa by a novel nanostructure modified carbon paste electrode. J Iran Chem Soc. 2011;9:27–34.
22. Zhao L, Li H, Gao S, Li M, Xu S, Li C, et al. MgO nanobelt-modified graphene-tantalum wire electrode for the simultaneous determination of ascorbic acid, dopamine and uric acid. Electrochim Acta. 2015;168:191–8.
23. Ouyang X, Luo L, Ding Y, Liu B, Xu D, Huang A. Simultaneous determination of uric acid, dopamine and ascorbic acid based on poly (bromocresol green) modified glassy carbon electrode. J Electroanal Chem. 2015;748:1–7.
24. Zheng X, Guo Y, Zheng J, Zhou X, Li Q, Lin R. Simultaneous determination of ascorbic acid, dopamine and uric acid using poly (l-leucine)/DNA composite film modified electrode. Sens Actuators B. 2015;213:188–94.
25. Zuo R, Zhou S, Zuo Y, Deng Y. Determination of creatinine, uric and ascorbic acid in bovine milk and orange juice by hydrophilic interaction HPLC. Food Chem. 2015;182:242–5.
26. Kaur B, Srivastava R. Simultaneous determination of epinephrine, paracetamol, and folic acid using transition metal ion-exchanged polyaniline–zeolite organic–inorganic hybrid materials. Sens Actuators B. 2015;211:476–88.
27. Ananthi A, Kumar SS, Phani KL. Facile one-step direct electrodeposition of bismuth nanowires on glassy carbon electrode for selective determination of folic acid. Electrochim Acta. 2015;151:584–90.
28. Beitollahi H, Hamzavi M, Torkzadeh-Mahani M. Electrochemical determination of hydrochlorothiazide and folic acid in real samples using a modified graphene oxide sheet paste electrode. Mater Sci Eng C. 2015;52:297–305.
29. Wang X, You Z, Cheng Y, Sha H, Li G, Zhu H, et al. Application of nanosized gold and graphene modified carbon ionic liquid electrode for the sensitive electrochemical determination of folic acid. J Mol Liq. 2015;204:112–7.
30. Kingsley MP, Desai PB, Srivastava AK. Simultaneous electrocatalytic oxidative determination of ascorbic acid and folic acid using Fe_3O_4 nanoparticles modified carbon paste electrode. J Electroanal Chem. 2015;741:71–9.
31. Abdelwahab AA, Shim Y-B. Simultaneous determination of ascorbic acid, dopamine, uric acid and folic acid based on activated graphene/MWCNT nanocomposite loaded Au nanoclusters. Sens Actuators B. 2015;221:659–65.
32. Shangguan E, Li Q. A pre-anodized inlaying ultrathin carbon paste electrode for simultaneous determination of uric acid and folic acid. Electrochim Acta. 2013;89:600–6.
33. Beitollahi H, Sheikhshoaie I. Electrocatalytic and simultaneous determination of isoproterenol, uric acid and folic acid at molybdenum (VI) complex-carbon nanotube paste electrode. Electrochim Acta. 2011;56:10259–63.
34. Kochana J, Gala A, Parczewski A, Adamski J. Titania sol–gel-derived tyrosinase-based amperometric biosensor for determination of phenolic compounds in water samples. Examination of interference effects. Anal Bioanal Chem. 2008;391:1275–81.
35. Wang Y, Hasebe Y. Acridine orange-induced signal enhancement effect of tyrosinase-immobilized carbon-felt-based flow biosensor for highly sensitive detection of monophenolic compounds. Anal Bioanal Chem. 2011;399:1151–62.
36. Tang L, Zeng G, Liu J, Xu X, Zhang Y, Shen G, et al. Catechol determination in compost bioremediation using a laccase sensor and artificial neural networks. Anal Bioanal Chem. 2008;391:679–85.
37. Sanz J, de Marcos S, Galbán J. Autoindicating optical properties of laccase as the base of an optical biosensor film for phenol determination. Anal Bioanal Chem. 2012;404:351–9.
38. Ghodsi J, Rafati AA, Shoja Y, Najafi M. Determination of dopamine in the presence of uric acid and folic acid by carbon paste electrode modified with CuO nanoparticles/hemoglobin and multi-walled carbon nanotube. J Electrochem Soc. 2015;162:B69–74.
39. Kafi AKM, Lee D-Y, Park S-H, Kwon Y-S. Potential application of hemoglobin as an alternative to peroxidase in a phenol biosensor. Thin Solid Films. 2008;516:2816–21.
40. Xiang Q, Meng G, Zhao H, Zhang Y, Li H, Ma W, et al. Au nanoparticle modified WO_3 nanorods with their enhanced properties for photocatalysis and gas sensing. J Phys Chem C. 2010;114:2049–55.
41. Badilescu S, Ashrit PV. Study of sol–gel prepared nanostructured WO_3 thin films and composites for electrochromic applications. Solid State Ionics. 2003;158:187–97.
42. Zheng H, Tachibana Y, Kalantar-zadeh K. Dye-sensitized solar cells based on WO_3. Langmuir. 2010;26:19148–52.

43. Chung Y-K, Kim M-H, Um W-S, Lee H-S, Song J-K, Choi S-C, et al. Gas sensing properties of WO_3 thick film for NO_2 gas dependent on process condition. Sens Actuators B. 1999;60:49–56.
44. Liu F, Li L, Mo F, Chen J, Deng S, Xu N. A catalyzed-growth route to directly form micropatterned WO_2 and WO_3 nanowire arrays with excellent field emission behaviors at low temperature. Cryst Growth Des. 2010;10:5193–9.
45. Ippolito SJ, Kandasamy S, Kalantar-Zadeh K, Wlodarski W. Hydrogen sensing characteristics of WO_3 thin film conductometric sensors activated by Pt and Au catalysts. Sens Actuators B. 2005;108:154–8.
46. Li H-Y, Cai Z-X, Ding J-C, Guo X. Gigantically enhanced NO sensing properties of WO_3/SnO_2 double layer sensors with Pd decoration. Sens Actuators B. 2015;220:398–405.
47. Lin Y, Huang L, Chen L, Zhang J, Shen L, Chen Q, et al. Fully gravure-printed NO_2 gas sensor on a polyimide foil using WO_3-PEDOT: PSS nanocomposites and Ag electrodes. Sens Actuators B. 2015;216:176–83.
48. Kim S, Park S, Park S, Lee C. Acetone sensing of Au and Pd-decorated WO_3 nanorod sensors. Sens Actuators B. 2015;209:180–5.
49. Kruefu V, Wisitsoraat A, Tuantranont A, Phanichphant S. Ultrasensitive H_2S sensors based on hydrothermal/impregnation-made Ru-functionalized WO_3 nanorods. Sens Actuators B. 2015;215:630–6.
50. Liu H, Duan C, Yang C, Chen X, Shen W, Zhu Z. A novel nitrite biosensor based on the direct electron transfer hemoglobin immobilized in the WO_3 nanowires with high length–diameter ratio. Mat Sci Eng C. 2015;53:43–9.
51. Deng Z, Gong Y, Luo Y, Tian Y. WO_3 nanostructures facilitate electron transfer of enzyme: application to detection of H_2O_2 with high selectivity. Biosens Bioelectron. 2009;24:2465–9.
52. Anik M, Cansizoglu T. Dissolution kinetics of WO_3 in acidic solutions. J Appl Electrochem. 2006;36:603–8.
53. Dawson G, Zhou W, Blackley R. Accelerated electron beam induced breakdown of commercial WO_3 into nanorods in the presence of triethylamine. Phys Chem Chem Phys. 2011;13:20923–6.
54. Wang Q, Das MR, Li M, Boukherroub R, Szunerits S. Voltammetric detection of L-dopa and carbidopa on graphene modified glassy carbon interfaces. Biogeosciences. 2013;93:15–22.
55. Reddaiah K, Reddy TM, Raghu P. Electrochemical investigation of L-dopa and simultaneous resolution in the presence of uric acid and ascorbic acid at a poly (methyl orange) film coated electrode: a voltammetric study. J Electroanal Chem. 2012;682:164–71.
56. Yaghoubian H, Karimi-Maleh H, Khalilzadeh MA, Karimi F. Electrocatalytic oxidation of levodopa at a ferrocene modified carbon nanotube paste electrode. Int J Electrochem Sci. 2009;4:993–1003.
57. Melo HCD, Seleghim APD, Polito WL, Fatibello-Filho O, Vieira IC. Simultaneous differential pulse voltammetric determination of L-dopa and carbidopa in pharmaceuticals using a carbon paste electrode modified with lead dioxide immobilized in a polyester resin. J Braz Chem Soc. 2007;18:797–803.
58. Nigović B, Jurić S, Mornar A, Malenica I. Electrochemical studies of ropinirole, an anti-Parkinson's disease drug. J Chem Sci. 2013;125:1197–205.